JMEPEG
https://doi.org/10.1007/s11665-018-3363-1

1059-9495/$19.00

# Corrosion Inhibition of Cold-rolled Low Carbon Steel with Pulse Fiber Laser Ablation in Water

*Sze Ney Chan, Wai Yin Wong, Rashmi Walvekar, Abdul Amir H. Kadhum, Mohammad Khalid, and Kean Long Lim*

*(Submitted May 15, 2017; in revised form March 27, 2018)*

**This study aims at the use of a fiber laser for modifying the surface properties of cold-rolled low carbon steel via a pulse laser ablation technique in water. The effect on the corrosion behavior of the fiber laser-treated metal surface was investigated in NaCl and HCl environments. Electrochemical tests showed significant improvement in the corrosion resistance of the laser-treated sample in NaCl, with an increase in open-circuit potential (OCP) from − 0.65 to − 0.60 V and an inhibition efficiency of 89.22% as obtained from the impedance study. Such improvement was less significant in an acidic environment. Lower corrosion rates of 20.9 mpy and 5.819 × $10^3$ mpy were obtained for the laser-treated samples in neutral and acidic electrolytes, respectively, than the corrosion rates obtained for the as-received samples (33.2 mpy and 11.98 × $10^3$ mpy). Morphological analysis indicated a passive film built by spherical grains of regular size on the metal surface after laser treatment. The corrosion inhibition effects in NaCl were evident by the nonexistence of the common corrosion products of lepidocrocite and crystalline structures that were seen on as-received samples; only polyhedral crystals with micrograins grown on them were seen covering the laser-treated surface. Therefore, the laser treatment using a fiber laser source improved the corrosion resistance of cold-rolled low carbon steel.**

**Keywords** cold-rolled low carbon steel, corrosion inhibition, fiber laser, pulse laser ablation in water

## 1. Introduction

In recent years, the manufacture of metallic materials for commercial applications has drawn significant interest among researchers. Metallic materials containing iron and aluminum have gained importance in the fields of electricity, medical therapy, and industrial equipment as well as in structural engineering. Metallic materials are known to have high structural strength per unit mass, high thermal and electrical conductivity, high reflectivity and high resistance to shear or deformation. However, there are certain properties such as inadequate strength and low resistivity to heat and corrosion that restrict the widespread application of metals for the structural uses (Ref 1). Meanwhile, fatigue, corrosion and wear failure of materials are common phenomena, implying that the materials are vulnerable to the environment and subsequently lose their original function.

Without doubt, mild steel is the essential class of metals. From low-end applications such as kitchenware, structural beams, and furniture to vehicles, the utilisation of carbon steels is necessary. Carbon steels are widely used throughout the world due to the good strength, desired ductility, ease of fabrication, availability, weldability and low cost. However, carbon steels are not perfect since they have less strong for their weight, are easily rusted and cannot be further improved by heat treatment, therefore resulting in the limitations for its wide applications. Despite these drawbacks, carbon steels are still widely used as the most economical materials of construction under different conditions.

Corrosion has been regarded as a main economic issue. According to the World Corrosion Organisation (WCO), it was estimated that the cost of corrosion worldwide was approximately $US 2.4 trillion annually, which is approximately 3% of the world's gross domestic product (GDP) (Ref 2). Various reported methods such as organic (Ref 3) and inorganic coatings (Ref 4) or surface modification (Ref 5) are used to extend the working life and corrosion resistance of metals under aggressive conditions.

Unforeseen corrosion issues will always occur, and it is a common challenge to prevent these occurrences. In many cases, the failure starts due to corrosion or fatigue. Previous research studies have shown that laser-based methods for surface modification offer significant improvements of the metal surface, attributed to the thermal effect and chemical reactions that could lead to the formation of novel microstructures and alloys (Ref 5). Over the last decade, substantial efforts have revealed important insights into a few areas that are related to laser-induced techniques such as laser surface melting, laser cladding, laser alloying and laser ablation, suitable for several applications: new material synthesis, nanoparticle synthesis, laser sampling for elemental analysis, etc. (Ref 6). Advanced technologies for alloying using ion implantation, electron beams and laser beams are able to synthesise a surface-modified layer that can delay corrosion. Yue et al. (Ref 7) reported a modified surface of Ti-6Al-4V alloy using an excimer laser to improve corrosion behavior for dental applications. Yue et al. revealed that the corrosion resistance

**Sze Ney Chan** and **Rashmi Walvekar**, School of Engineering, Taylor's University Lakeside Campus, Jalan Taylor's, 47500 Subang Jaya, Selangor, Malaysia; **Wai Yin Wong, Abdul Amir H. Kadhum,** and **Kean Long Lim**, Fuel Cell Institute, University Kebangsaan Malaysia, 43600 Bangi, Selangor, Malaysia; and **Mohammad Khalid**, Research Centre for Nano-Materials and Energy Technology, School of Science and Technology, Sunway University, No. 5, Jalan Universiti, Bandar Sunway, 47500 Subang Jaya, Selangor, Malaysia. Contact e-mails: waiyin.wong@ukm.edu.my and rashmigangasa.walvekar@taylors.edu.my.



Published online: 20 April 2018

in the alloys increased by a factor of 7 compared to that of the original alloy.

Pan et al. (Ref 8) showed that laser ablation of carbon fiber-reinforced polymer (CFRP)/magnesium alloy laminates using a pulsed ytterbium fiber laser system offered excellent protection against corrosion because the corrosion rate for the laser-treated sample decreased by 80%, giving a value of 0.040 mg $cm^{-2}$ $h^{-1}$ compared to the grit blasted sample value of 0.226 mg $cm^{-2}$ $h^{-1}$. Peyre et al. (Ref 9) also agreed that surfaces of 316L steel ablated by a Nd/glass laser are preserved from corrosion by a protective layer attributed to the surface modification on the rear face of the coating via thermal treatment. Similar findings were claimed by Lee et al. (Ref 10) on the effect of surface modification on the corrosion performance of AISI 304 stainless steel, where the corrosion potential of the laser shot-peened sample rose from − 275 to − 248 mV, and the current density declined from 26.3 to 5.2 μA/$cm^2$. Lu et al. (Ref 11) reported that compressive residual stress is beneficial in inhibiting stress corrosion cracking (SCC) initiation in the corrosive solution containing chloride ions where uniform corrosion pits of approximately 2.5-2 μm were observed at the top surfaces of the laser-treated samples compared with those of the as-machined sample, which had non-uniform corrosion pits measuring approximately 20-35 μm.

Among the laser-induced techniques, pulse laser ablation in liquid has emerged as one of the cleanest and safest methods to perform a role similar to laser shock peening. PLAL takes advantage of providing a rapid cooling effect in the workpiece after the pulsed laser beam strokes on the metal surface. This method was found to enhance the surface properties such as corrosion behavior, surface morphology and hardness properties due to the thermal effect and was expected to increase the compressive residual stress on the metal surface. In the past, the Nd-YAG laser (Ref 12), excimer laser (Ref 7) or $CO_2$ laser (Ref 5) have been more widely used for the abovementioned work, with positive results. To our best knowledge, the fiber laser has yet to be studied regarding the investigation of corrosion behavior. Because the fiber laser is relatively more environmentally safe and practical to be utilised (Ref 13), this study aimed to investigate its use to modify the metal surface and subsequently to study its corrosion resistance effects on ASTM A1008 cold-rolled low carbon steel.

## 2. Materials and Methods

### 2.1 Materials

Metal targets used in this study included ASTM A1008 cold-rolled low carbon steel, having a dimension of 6 × 4 cm with a thickness of 1.2 mm. The composition (wt.%) of the metallic steel was determined using arc-spark optical emission spectroscopy (WAS Foundry-Master, Oxford Instruments) with the following results: Fe, 99.5; Mn, 0.16; C, 0.06; and Al, 0.03, with traces of Si, P, S, Co, Ni and Cu. Sodium chloride (NaCl) of 99% purity was obtained from R&M Chemicals. Ethyl alcohol ($C_2H_5OH$) with 95% of purity and acetone ($CH_3COCH_3$) with a purity of 99.5% were also obtained from R&M Chemicals for sample cleaning. In addition, an alumina suspension with a particle size of 0.05 μm was purchased from Buehler, for metal polishing purposes.

### 2.2 Sample Preparation

The surfaces of the test specimens were polished with SiC abrasive paper (grit value of 500-2000) to ensure smooth and even surfaces that are free from mold contaminants. Subsequently, the sample targets were fine-polished with 0.05 μm alumina suspension in accordance with ASTM standard E3-11. Ultrasonic cleaning of metal targets was performed sequentially with acetone and ethanol using Crest 5 Gallon Heated Ultrasonic Cleaner (4HT-1014-6, Crest Ultrasonics Corp.) for 20 min at 50 °C; the targets were then air-dried before storing. Before the laser irradiation, all the samples were again cleaned with acetone and ethanol.

### 2.3 Experimental Setup

Laser ablation was conducted using a pulsed mode ytterbium-doped fiber laser (YLP-1-100-20-20-HC, IPG Photonics) with a maximum output power of 21 W and with the output characteristics of 1064 nm wavelength and a pulse width of ∼ 100 ns. A vertical configuration was utilised for PLAL experiments to direct and focus the laser beam downward onto the metal targets. The metal target was placed on a Perspex block in an 800-ml glass beaker filled with ultrapure water, covering the metal target surface to a depth of 5 mm. Ultrapure water was used to ensure that no contaminant deposition occurred on the metal surface after the laser ablation while assisting rapid quenching of the laser-shocked surface. The glass beaker was fixed on a *x*–*y* motion stage (micropositioner) for experimental displacement. Typically, the laser treatment conditions used to treat 6 × 4 cm rectangular metal targets were the following: overlap rate, 60%; scanning speed, 2000 mm/s; power of laser irradiation, 4.2 W; number of laser pulses, 100,000; and with an active impact diameter of 50 μm. After the laser ablation experiment, the metal targets were wiped with a clean paper and air-dried. The laser-ablated metal targets obtained were stored tightly in a moisture-free storage box.

### 2.4 Sample Characterisation

**2.4.1 Electrochemical Corrosion Testing.** Corrosion behavior of the samples was evaluated based on potentiodynamic polarisation in 3.5 wt.% NaCl and 10% HCl solutions at 25 °C using a potentiostat (Gamry Instrument Potentiostat/Galvanostat/ZRA model Ref. 600). A conventional three-electrode setup was used for the corrosion testing with the working, counter and the reference electrodes of test metal samples, graphite electrode and saturated calomel electrode (SCE), respectively. The metal samples used were briefly polished with 0.05 μm alumina suspension and subsequently degreased with acetone and ethanol for 10 min in an ultrasonic bath as per ASTM G1-03 prior to the tests. The surface of the laser-treated or as-received sample was mounted into the corrosion cell setup with an exposed area of 1.0 $cm^2$. The working electrode was exposed to the electrolyte solution. During the test, open-circuit potential (OCP) was carried out initially for 3 h to reach potential stabilisation. Second, electrochemical impedance spectroscopy (EIS) was performed over a frequency range of 10 kHz-0.01 Hz in NaCl solution and 10 kHz to 0.1 Hz in HCl solution, with a signal amplitude perturbation of 10 mV. Subsequently, the electrochemical measurement was taken. The potentiodynamic polarisation

(PDP) measurement was taken after another OCP measurement from − 500 to 500 mV (SCE) at a scan rate of 0.5 mV/s to ensure that the former potential achieved a stable value before the test. The values of corrosion potential ($E_{corr}$) and corrosion current density ($I_{corr}$) were calculated from the intersection of the cathodic and anodic Tafel curves extrapolated from the cathodic and anodic polarisation curves. To ensure the accuracy of the experimental results, three repetitions were performed to characterise each sample to obtain an average value of the corrosion potential.

**2.4.2 Optical Microscope and Scanning Electron Microscope.** The surface morphology of the specimens was observed using an optical microscope (OM) (Olympus Ltd., BX51M). The surface morphology and the elemental composition of the samples were studied using a field emission scanning electron microscope (FESEM) equipped with energy dispersive spectrometer (EDX) (FEI Model, Quanta 400F) at a current beam of 1.1 nA, a beam voltage of 10 kV and scanning magnification of 120-20,000 times. The surface of the samples was cleaned ultrasonically with acetone and ethanol, sequentially, before the analysis.

**2.4.3 X-ray Diffraction (XRD).** A high-angle x-ray diffractometer (Bruker/D8 Advance) equipped with Ni-filtered Cu Kα radiation was used to examine the crystallographic structure of the as-received and laser-treated metal target surface. The XRD was measured within the 2$\theta$ range of 20°-90° with an accelerating voltage of 40 kV and a current of 40 mA. The grazing incidence technique was adopted to provide crystallographic information of the surface.

## 3. Results and Discussion

### 3.1 Electrochemical Measurement

Figure 1 presents the OCP of cold-rolled low carbon steel with time immersed in 3.5 wt.% NaCl and 10% HCl solutions at 25 °C for 3 h. The OCP values were observed to vary over time. The OCP of the cold-rolled low carbon steel underwent a cathodic drop at the beginning of immersion in NaCl solution, as shown in Fig. 1(a). This cathodic drop indicated the weakening of the oxide constituted on the metal surface due to removal of the thin surface oxides (Ref 14). For the as-received sample in NaCl solution, the OCP after stabilisation was observed to be − 593.85 mV (± 6.3 mV). After PLAL treatment, the OCP after stabilisation reached approximately − 531.65 mV (± 5.7 mV). A more positive OCP value of 62.2 mV was observed on the laser-treated sample. Both samples in NaCl solution depicted a slight rise in the corrosion potential approximately at 550 s, but it showed a withdrawal at the end of the measurement. This initial rise was ascribed to the possible formation or thickening of the oxide film on the metal surface, which could enhance the corrosion protection ability of the metal target (Ref 15). In addition, this potential rise also indicated that a film was grown on the surface of the sample in the solution, likely due to the formation of rust.

When the samples were measured in a more corrosive environment using HCl as an electrolyte as shown in Fig. 1(b), the rise was apparent for both samples at the beginning. This rise in OCP values depicted the growth of a protective layer on the surface of the sample in the corrosive solution. Meanwhile, intensive fluctuation in the corrosion potential appeared during the immersion since a more corrosive solution (10% HCl solution) was employed than NaCl solution. The OCP exhibited on the laser-treated sample in HCl solution reached an average stationary OCP value of 12.85 mV more positive than the as-received sample, similar to the trend observed in the NaCl solution.

From Fig. 1, the laser-treated sample showed a better tendency for electrochemical oxidation in terms of rising curves in the HCl solution than in the NaCl solution. The effect of laser treatment appears to have created a layer of surface oxides acting as a passivation layer (Ref 15), making the anodic process control the electrode surface.

The corrosion resistances of the laser-treated and as-received cold-rolled low carbon steels were further verified using impedance measurement represented by Nyquist plots for the samples immersed in 3.5 wt.% NaCl solution and 10% HCl solution, as shown in Fig. 2. Both Nyquist plots of the samples showed capacitive loops that are associated with the charge transfer during the corrosion process in the oxide film covering the electrode surface (Ref 16).

The phase angle Bode plot is widely implemented to analyze the CPE exponent (Ref 17). Figure 3 shows that the laser-treated samples that gave values of phase angle close to 60° and a more negative value illustrated a good corrosion inhibitive nature owing to the rise in the protection layer on the ablated surface. Moreover, the rise in phase angle at the relaxation frequency occurred on the laser-treated sample in comparison with the as-received sample represented that the capacitive output increased with the superior effect of laser treatment. In addition, there was an increase in the absolute impedance values at lower frequencies for the laser-treated samples, which is explained because there was higher surface protection. The increase in absolute impedance values was believed to be related to the effect of a passivating layer that restricted the chemical reaction between the metal surface and the corrosive medium.

To further interpret the electrochemical behavior of carbon cold rolled steel in two different corrosive environments, an equivalent circuit was used to fit the data (shown in Fig. 2) (Ref 18). The Bode plots in Fig. 3 show only one loop, suggesting that one time constant is used. The components in the equivalent circuit include the following: the solution resistance ($R_s$), charge transfer resistance ($R$ct) and the constant phase element of double layer ($CPE_{dl}$). The corroding surface of steel in corrosive solution was believed to be non-homogeneous due to the induced roughness after laser treatment; hence, a CPE was implemented instead of a pure capacitor to denote the non-ideal capacitive behavior of the corrosion system, attributed to the induced dispersion effects that occurred on the metal surface (Ref 19). The impedance of CPE is given in Eq 1 (Ref 19).

$$Z_{CPE} = Y_0^{-1}(jw)^{-n} \quad \text{(Eq 1)}$$

where $Y_0$ is the magnitude of the CPE and $n$ is an empirical exponent between 0 and 1. The variation of $n$ is included to take in consideration of the heterogeneity of the surface. When $n = 1$, the CPE represents a pure capacitor. However, for a corrosion system, $n$ has a value between 0 and 1 that relies on the surface roughness of the surface.

The equivalent circuit component values were obtained and are tabulated in Table 1. To validate the polarisation result, the inhibition efficiency (I.E.%) of carbon cold rolled steel in 3.5

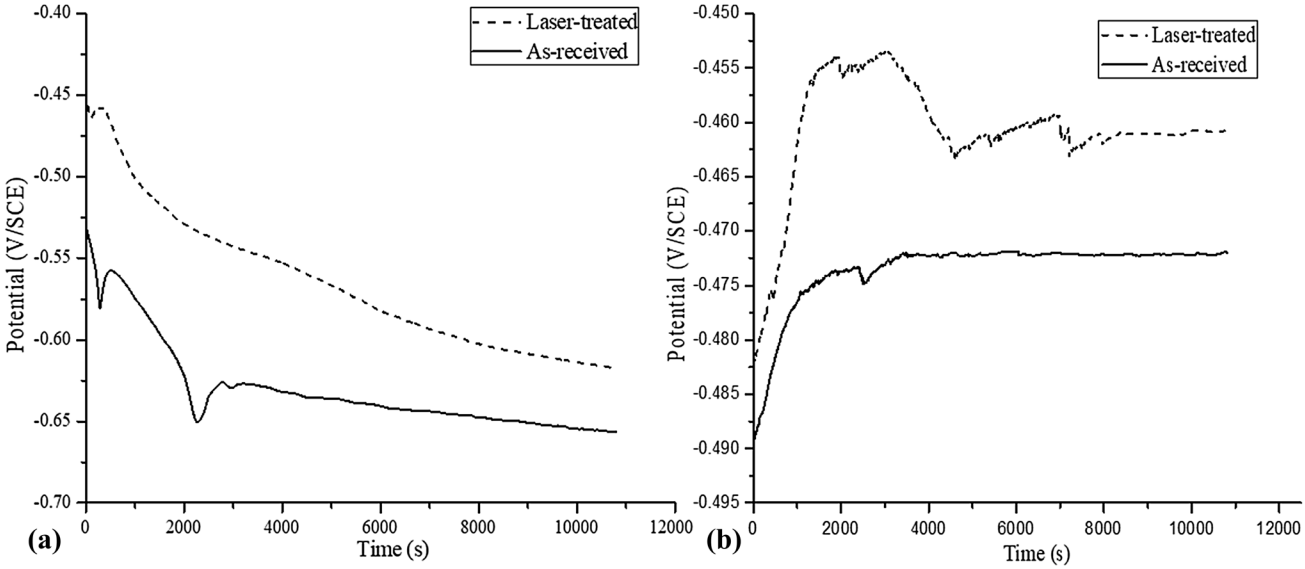


**Fig. 1** OCP-time curves of the as-received and laser-treated cold rolled carbon steel samples in: (a) 3.5 wt.% NaCl and (b) 10% HCl solutions

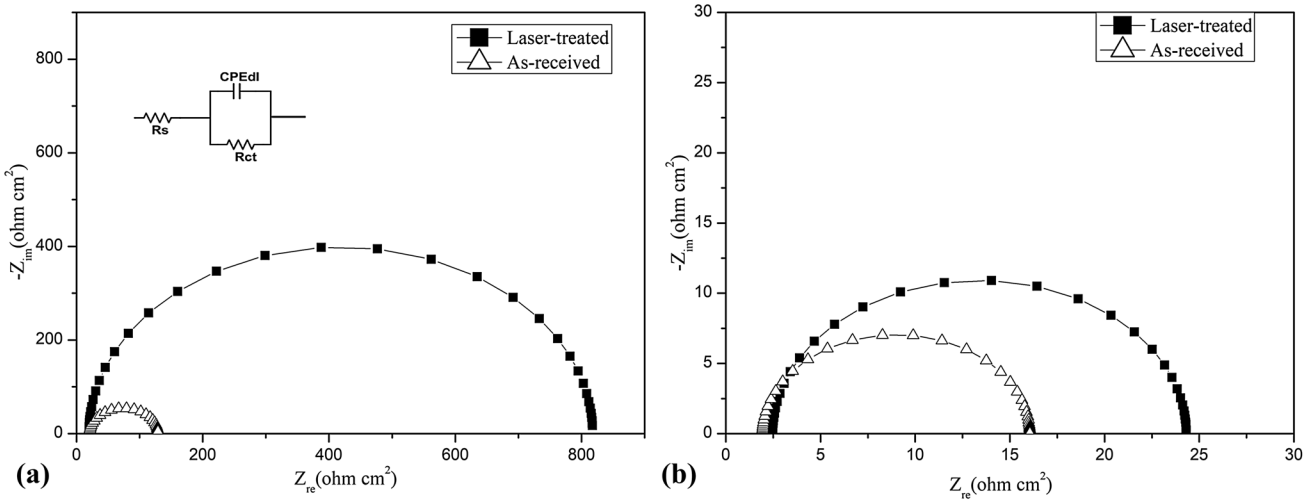


**Fig. 2** Nyquist plots of the EIS responses of the laser-treated and as-received cold rolled carbon steels in (a) 3.5 wt.% NaCl and (b) 10% HCl solutions and the equivalent circuit model used to fit the impedance data

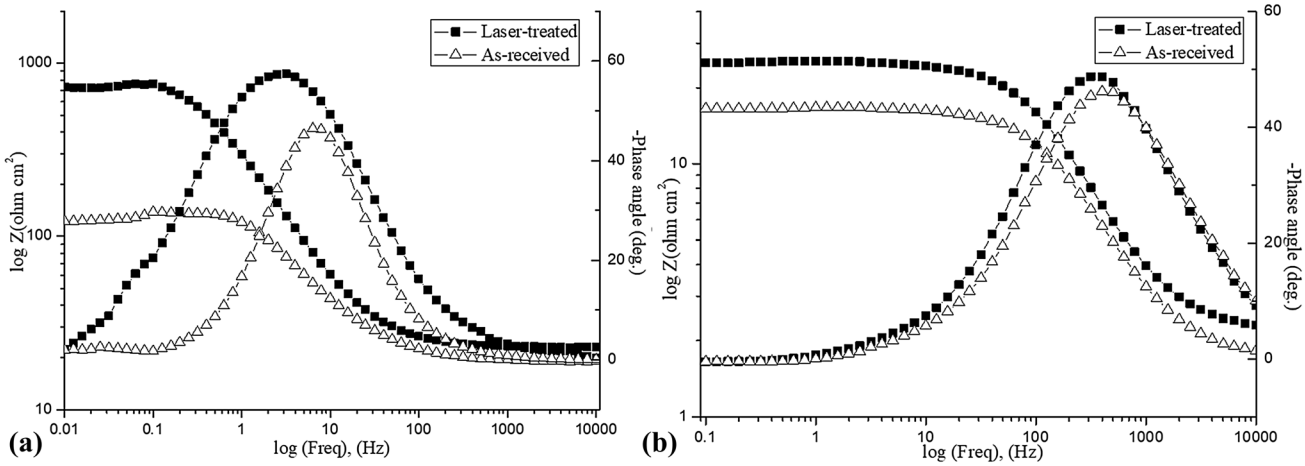


**Fig. 3** The experimental impedance and phase data in Bode plots for cold rolled carbon steels in (a) 3.5 wt.% NaCl and (b) 10% HCl solutions and an equivalent circuit to fit the impedance data

**Table 1 Electrochemical impedance parameters and inhibition efficiency of carbon cold rolled steel in 3.5 wt.% NaCl and 10% HCl solutions**

| Sample | $R_{ct}$, Ω cm$^2$ | $R_s$, Ω cm$^2$ | $CPE_{dl}Y_0$, Ω$^{-1}$ cm$^{-2}$ | I.E.% |
|---|---|---|---|---|
| 3.5 wt.% NaCl solution | | | | |
| Laser-treated | 798.0 (± 31.75) | 19.83 (± 2.68) | $5.36 \times 10^{-4}$ (± 1.745) | 86.38 |
| As-received | 108.7 (± 1.03) | 20.56 (± 0.006) | $4.32 \times 10^{-4}$ (± 0.106) | |
| 10% HCl solution | | | | |
| Laser-treated | 21.84 (± 1.18) | 2.479 (± 0.017) | $6.89 \times 10^{-5}$ (± 0.01) | 35.39 |
| As-received | 14.11 (± 1.87) | 1.947 (± 0.259) | $7.91 \times 10^{-5}$ (± 0.095) | |

wt.% NaCl and 10% HCl solution is computed from the relevant electrochemical impedance data according to Eq 2 (Ref 20).

$$\text{I.E.}\% = \frac{R_{ct} - R_{ct}^{o}}{R_{ct}} \times 100 \quad \text{(Eq 2)}$$

where $R_{ct}$ and $R_{ct}^{o}$ are the charge transfer resistances with respect to laser-treated and as-received samples, respectively, obtained from the curve fitting.

As for the laser-treated and as-received samples in 3.5 wt.% NaCl solution, the value of $R_{ct}$ of the laser-treated sample appears to be approximately seven times the value of $R_{ct}$ for the as-received sample, which was attributed to the increase in the inhibition efficiency. This increase in the $R_{ct}$ value observed on the laser-treated sample signified the resistance of the metal surface to electrochemical reaction. The surface-modified layer was able to restrict chemical reaction between the metal surface and a corrosion medium (Ref 21). Nonetheless, no distinct difference in corrosion resistance was observed in the HCl solution, likely attributed to the ineffectiveness of the passive film to protect the metal in a harsher environment. Overall, EIS showed that the enhancement in corrosion resistance of laser-treated cold rolled steel was significant in neutral solution.

Muralisankar et al. (Ref 22) reported that the highest I.E.% in 3.5 wt.% NaCl of the mild steel was obtained at 61.82% with the addition of *N*(1)-pentyl isatin-*N*(4)-methyl-*N*(4)-phenyl thiosemicarbazone (PITSc) as a corrosion inhibitor. In this study, the highest I.E.% of the laser-treated carbon cold rolled steel in 3.5 wt.% NaCl was 86.38%, displaying a higher efficiency than in the abovementioned study.

Figure 4 represents the potentiodynamic polarisation of the laser-treated and as-received carbon cold rolled steel in 3.5 wt.% NaCl and 10% HCl solutions at 25 °C. After applying cathodic polarisation, the laser-treated samples exhibited a shift in $E_{corr}$ toward a more noble direction and a decrease in the $I_{corr}$ value in both corrosion media. The corrosion potential ($E_{corr}$) and the corrosion current ($I_{corr}$) extracted from the curves for both conditions (neutral and acidic solutions) are summarised in Table 2. An improvement in $E_{corr}$ value was observed when the steel was immersed in the NaCl medium, with a positive shift from − 0.70 to − 0.54 V. This phenomenon may be attributed to the formation of a very thin film that inhibits the attack of $Cl^-$ ions (from NaCl solution) into the surface. The shift in this value was found less significant in the harsher environment, implying no apparent improvement in corrosion resistance was observed after laser treatment. This result further correlates with the impedance data. According to Cui et al. (Ref 23), there is the presence of oxides and fine grains formed after PLAL treatment, leading to enhancement in different corrosion properties, as observed by a noble shift in the corrosion potential value. These compact oxide layers can act as a protective barrier to protect the carbon cold rolled steel against corrosion. Owing to the additional heat treatment on the overlapping laser spot, there was appreciable change in the microstructure and chemical composition of the metal surface (Ref 24). A similar observation was found in this study, and it will be explained through the XRD and SEM results in the later section.

The observation of $E_{corr}$ for laser-treated cold rolled steel in the present study was more positive than the observation of $E_{corr}$ reported by Singh et al. (Ref 25) for J55 carbon steel in 3.5% NaCl solution with a macrocyclic inhibitor, where the most positive $E_{corr}$ was approximately − 744 mV. It was calculated that via the fiber laser PLAL technique, the corrosion rate was reduced by 37.0 and 51.3% compared to that of the as-received carbon cold rolled steel in 3.5 wt.% NaCl and 10% HCl solutions, respectively. Musa et al. (Ref 26) reported that the largest displacement of $E_{corr}$ in their experiment under acidic conditions was approximately 12 mV for all inhibitors studied, less than that in the present study, which had an improvement of 26 mV.

### 3.2 Physicochemical Characterisation

**3.2.1 Before Corrosion.** Figure 5 shows the optical micrographs of the as-received and laser-treated sample surface. Periodic laser scanning tracks were observed on the laser-treated surface, as shown in Fig. 5(b). The tracks resulted from the laser irradiation on the cold rolled steel surface with overlapping rate of 60% and repetitive pulse frequency of 100 kHz. Hence, it is confirmed that the fiber laser pulse ablation has sufficient energy to eject a macroscopic amount of metal atoms from the cold rolled steel surface and to form an ordered pattern on it.

Scanning electron microscopy was subsequently used to study the surface morphology of the samples before and after corrosion tests. The microstructures of the cold-rolled samples before and after laser treatment are shown in Fig. 6. Figure 6(b) shows that a layer of spherical grains of regular size was formed on the surface of the laser-treated steel surface. Iron oxides are suspected to be formed on the surface during the laser ablation process. Due to the high energy gained from the laser ablation, there is a possibility that the iron particles are ionised and react with dissolved oxygen in water to form layers of iron oxides. According to Antonov et al. (Ref 27), who have performed Nd/glass laser treatment on cold-rolled low carbon mild steel, the oxide film formed on the surface consisted of two monophasic layers, i.e. $Fe_3O_4$ and FeO.

Unfortunately, the phases of iron oxides formed on the sample surface in this study are not detectable with XRD

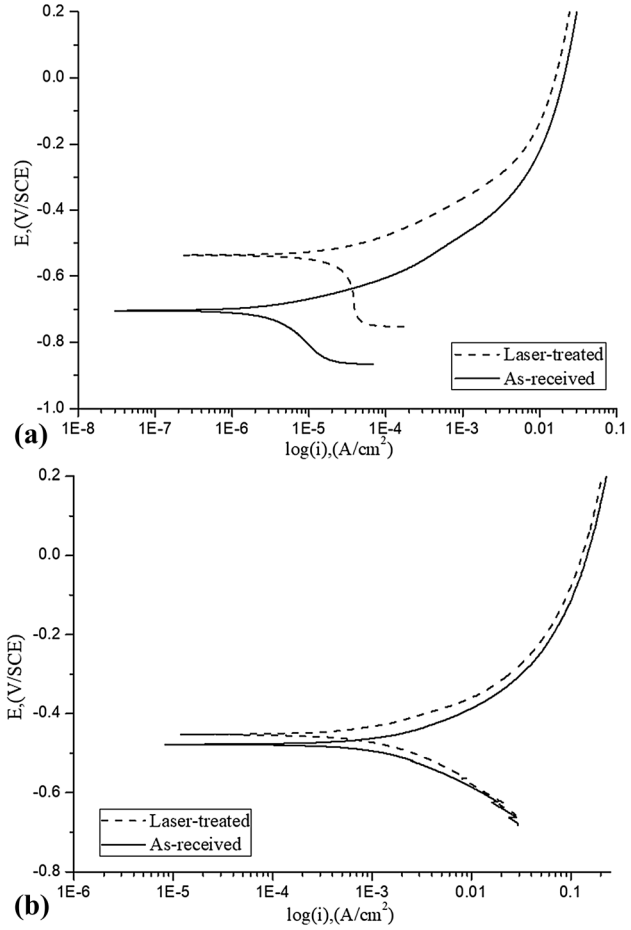


**Fig. 4** Polarisation curve of the as-received and laser-treated samples immersed in (a) 3.5 wt.% NaCl and (b) 10% HCl solutions

(Fig. 7), owing to the limitation of the grazing-incidence technique, which has a poor signal-to-noise ratio (Ref 27). Nonetheless, there are still correlations between the XRD results and the morphology changes in SEM. The diffraction peaks at 45.3°, 65.3° and 83.1° of the as-received sample indicate the presence of an alpha-Fe phase, which is commonly found in cold rolled steels (Ref 28). There is no additional peak observed upon laser treatment. However, the laser-treated sample increases in peak intensity at 45.3°, suggesting that laser treatment could enhance the formation of alpha-Fe. The morphology in Fig. 6(b) correlates with this observation, in which it appears that many of the spherical grains contain black nodules at the center of the sphere. It is suggested that during the ejection of metal surface atoms by laser ablation, the new surfaces are heated up rapidly; nonetheless, water quenches the surface to room temperature concurrently and suppresses the precipitation of carbon, causing the formation of a supersaturated alpha-Fe solid solution region. Upon natural aging, carbon slowly precipitates from the carbon-enriched region and forms gray iron and graphite (appeared as black nodules) (Ref 29). In addition, a slight shift of the $2\theta$ angle to a higher angle was observed at 65.3°, indicating that the lattice of the BCC alpha-Fe contracts after laser treatment, which is possibly caused by the carbon atoms precipitating from the iron lattice. From the microstructural observations of both SEM and XRD, we could postulate that the enhancement of corrosion resistivity of the laser-treated sample was due to the formation of graphite.

**Table 2 The results of a potentiodynamic corrosion test in 3.5 wt.% NaCl and 10% HCl solutions**

| Sample | 3.5 wt.% NaCl solution | | | 10% HCl solution | | |
|---|---|---|---|---|---|---|
| | Corrosion potential in, $E_{corr}$, mV | Corrosion current density, $I_{corr}$, μA/cm$^2$ | Corrosion rate, mpy | Corrosion potential, $E_{corr}$, mV | Corrosion current density, $I_{corr}$, mA/cm$^2$ | Corrosion rate, mpy |
| Laser-treated | − 536 | 46.3 | 20.9 | − 452 | 12.9 | $5.819 \times 10^3$ |
| As-received | − 706 | 73.5 | 33.2 | − 478 | 26.5 | $11.98 \times 10^3$ |

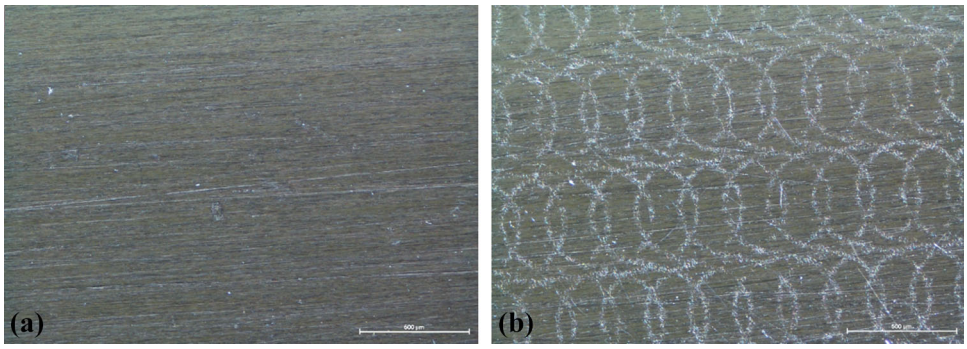


**Fig. 5** Image of metal plate of the (a) as-received sample and (b) laser-treated sample

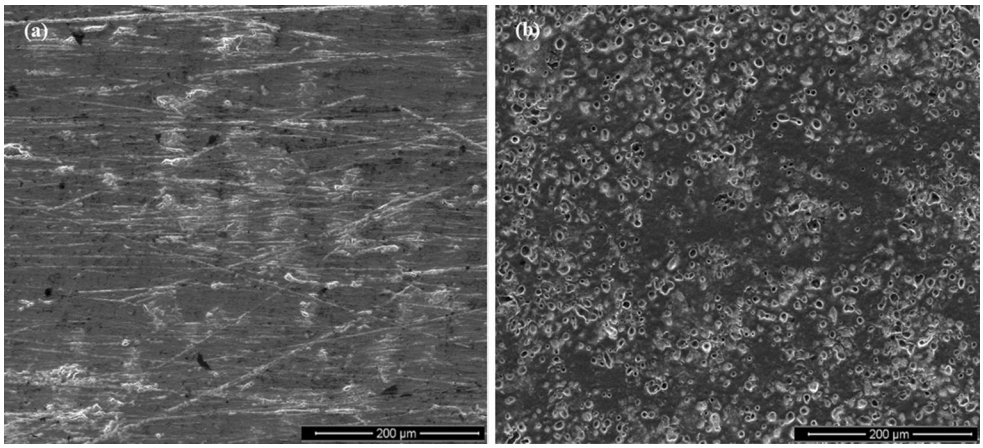


**Fig. 6** Surface micrographs of the (a) as-received sample and (b) laser-treated sample at a magnification of 500×

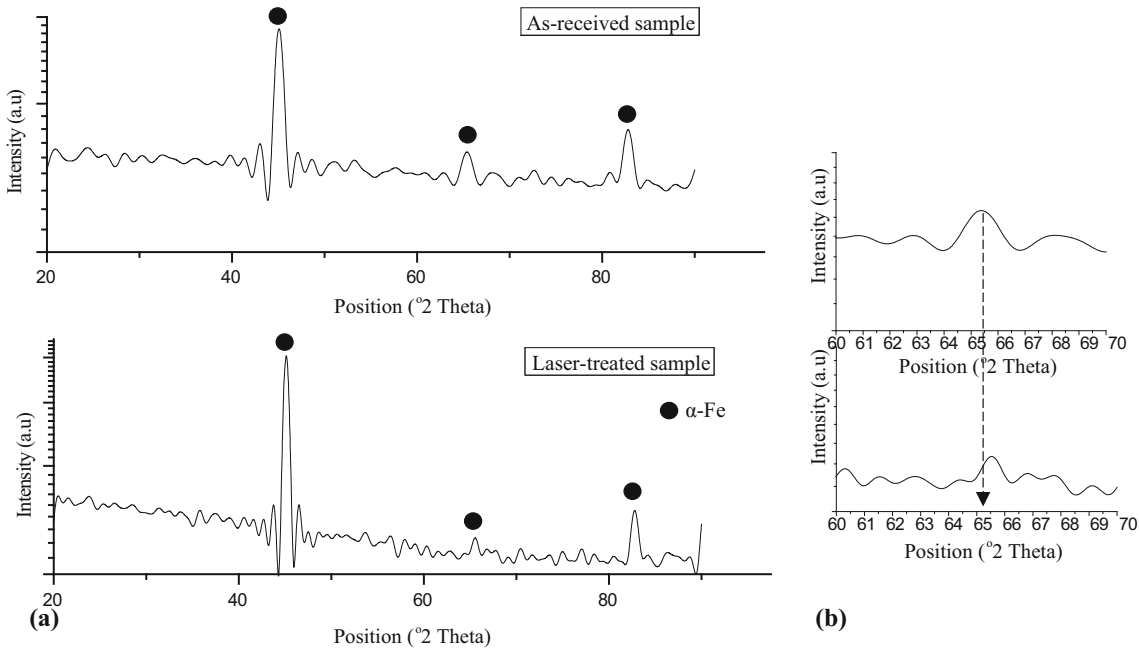


**Fig. 7** XRD spectra in grazing incidence of (a) as-received and laser-treated samples, and (b) magnified region of XRD spectra shown in (a)

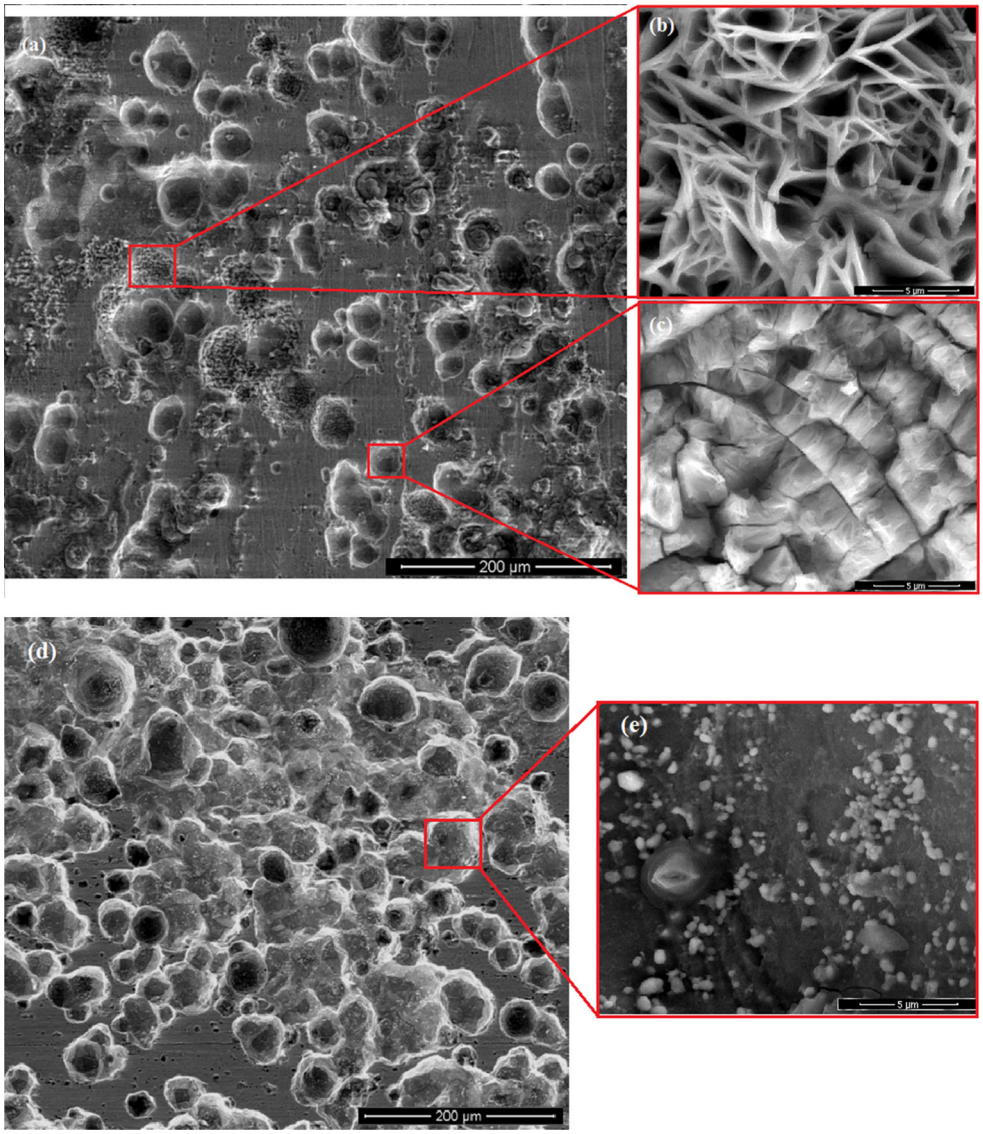


**Fig. 8** Corroded surface after the corrosion test in NaCl electrolyte: the as-received sample showing the (a) polyhedral and "cotton-like" spherical structure, (b) higher magnification with lepidocrocite structure, (c) higher magnification with crystalline structure; and the laser-treated sample showing the (d) polyhedral crystal structure and (e) higher magnification with micrograins shown on the polyhedral crystal surface

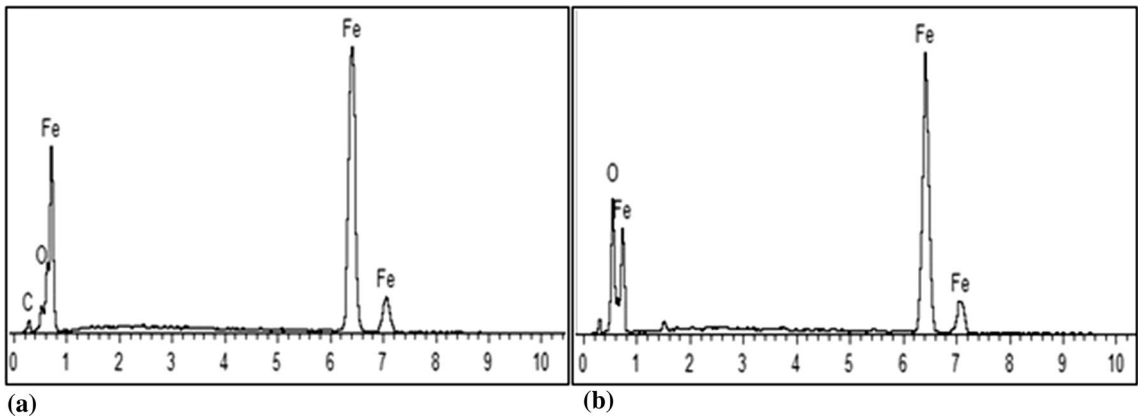


**Fig. 9** EDX spectra of the (a) as-received and (b) laser-treated carbon cold rolled steel samples after the corrosion test in NaCl medium

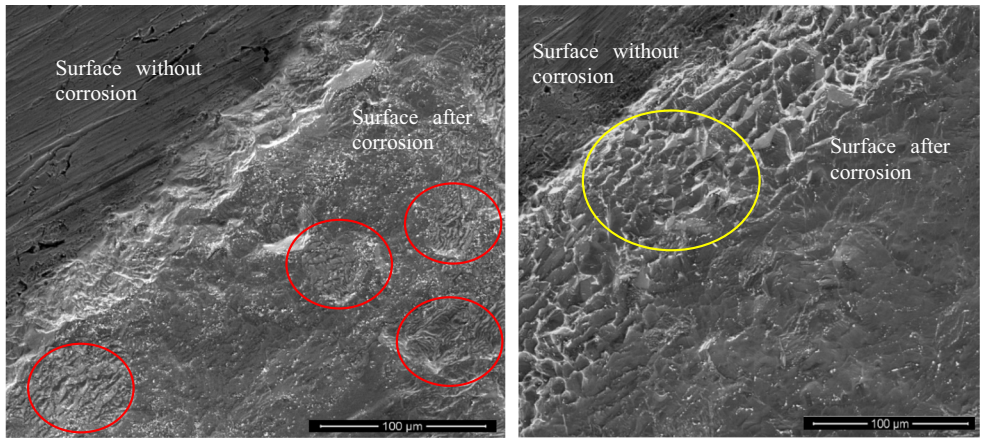


**Fig. 10** Surface morphology after electrochemical testing in HCl medium of the (a) as-received sample showing many micrograins and corrosion spots with a porous structure (circle in red) and the (b) laser-treated sample showing a multilayer flake-like structure with fewer micrograins (circle in yellow) (Color figure online)

**3.2.2 After Corrosion.** Figure 8 shows the surface morphologies of the laser-treated and as-received samples after the corrosion tests in NaCl. As observed, the as-received sample showed more exposed bare metal surface (Fig. 8a), and its corrosion products were in the form of "cotton-ball"-structured lepidocrocite (Fig. 8b) and polyhedral crystalline spheres (Fig. 8c) (Ref 30). Rust formation was evident by the detection of a "cotton-ball" structure with a high porous structure. In contrast, the corrosion product of the laser-treated sample consisted mainly of densely packed layers of polyhedral crystalline structure bounded by high-index facets, as shown in Fig. 8(d) and (e). The corrosion products were mostly in spherical shape, where the laser-treated sample had a higher packing structure than that of the as-received sample. The EDX results in Fig. 9 also confirm that these polyhedral spheres are iron oxide, that is, the laser-treated sample has a higher oxygen concentration than does the as-received sample. These polyhedral spheres oxide are suggested to be in the form of magnetite ($Fe_3O_4$), which would be the final form of the oxide product on carbon steels, as proposed by Momber (Ref 31). Magnetite is commonly known as a protective metal oxide film that acts as a barrier against corrosion, which passivates and retards iron atoms from further corrosion due to its low solubility under moist conditions (solubility in aqueous environment is a measure of stability) (Ref 31). Corresponding to the OCP trends in the previous section, the sudden increase in the OCP is suggested to be where the magnetite starts to form, grow and eventually cover the surface of the metal (when OCP reaches a steady value). In short, controlling the amount of polyhedral crystalline spheres, which can be controlled by laser treatment, is essential in improving the corrosion resistivity of cold-rolled steel in the NaCl medium.

Figure 10 shows the surface morphologies of the samples after immersion in the HCl medium and shows that the morphology of the corrosion surface is highly influenced by the medium. When the samples were subjected to a more corrosive HCl medium, no polyhedral structure was found. Instead, dense layers of corrosion products were observed on both the as-received and laser-treated samples, possibly attributed to the different corrosion pathways in different media. Although the electrochemical tests (in section 3.1) of cold-rolled steel in HCl have shown a better corrosion resistivity upon laser treatment, the improvement is incremental compared to the results from the NaCl medium. Therefore, the morphology differences in corrosion products between the as-received and laser-treated samples are expected to be less pronounced. Nonetheless, the laser-treated sample shows multilayer flake-like brittle structures at the edge of corrosion, whereas the corrosion products of the as-received sample had more porous structures. The flake-like structures are the results of surface hardening by the laser treatment, where the melting and quenching process produces hard and corrosion-resistant martensitic microstructures as a protective layer (Ref 32). In other word, laser treatment can be used to produce a localised corrosion protective layer at the target area.

## 4. Conclusions

This study demonstrated that a fiber laser can modify the surface properties of cold-rolled low carbon steel through a pulse laser ablation technique in water. The results showed that the corrosion resistance was significantly improved when the laser-treated sample was subjected to the NaCl environment, with an improved corrosion potential that is 70 mV higher than that of the as-received sample, with 89% inhibition efficiency. The improvement was shown to result from the formation of a passive film that acts as a protective barrier.


## Acknowledgments

This work is supported by Universiti Kebangsaan Malaysia (DIP-2016-020 and GUP-2015-034). The authors are grateful to the Center for Research and Instrumentation, UKM, for the support on the x-ray diffraction (XRD) characterisation of the metal plate.


## References


1. Y. Wan, G. Xiong, H. Luo, F. He, Y. Huang, and Y. Wang, Influence of Zinc Ion Implantation on Surface Nanomechanical Performance and

Corrosion Resistance of Biomedical Magnesium–Calcium Alloys, *Appl. Surf. Sci.*, 2008, **254**, p 5514–5516
2. J. Velázquez, J. Van Der Weide, E. Hernández, and H.H. Hernández, Statistical Modelling of Pitting Corrosion: Extrapolation of the Maximum Pit Depth-Growth, *Int. J. Electrochem. Sci.*, 2014, **9**, p 4129–4143
3. M. Bahrami, S. Hosseini, and P. Pilvar, Experimental and Theoretical Investigation of Organic Compounds as Inhibitors for mild Steel Corrosion in Sulfuric Acid Medium, *Corros. Sci.*, 2010, **52**, p 2793–2803
4. R. Figueira, C.J. Silva, and E. Pereira, Organic–Inorganic Hybrid Sol–Gel Coatings for Metal Corrosion Protection: A Review of Recent Progress, *J. Coat. Technol. Res.*, 2015, **12**, p 1–35
5. W.R. Osório, N. Cheung, L.C. Peixoto, and A. Garcia, Corrosion Resistance and Mechanical Properties of an Al 9 wt% Si Alloy Treated by Laser Surface Remelting, *Int. J. Electrochem. Sci.*, 2009, **4**, p 820–831
6. V.N. Lednev, S.M. Pershin, A.A. Ionin, S.I. Kudryashov, S.V. Makarov, A.E. Ligachev et al., Laser Ablation of Polished and Nanostructured Titanium Surfaces by Nanosecond Laser Pulses, *Spectrochim. Acta Part B*, 2013, **88**, p 15–19
7. T.M. Yue, J.K. Yu, Z. Mei, and H.C. Man, Excimer Laser Surface Treatment of Ti-6Al-4V Alloy for Corrosion Resistance Enhancement, *Mater. Lett.*, 2002, **52**, p 206–212
8. Y. Pan, G. Wu, Z. Huang, Z. Zhang, H. Ye, M. Li, and S. Ji, Improvement in Interlaminar Strength and Galvanic Corrosion Resistance of CFRP/Mg Laminates by Laser Ablation, *Mater. Lett.*, 2017, **207**, p 4–7
9. P. Peyre, X. Scherpereel, L. Berthe, R. Fabbro, G. Beranger, and C. Lemaitre, Surface Modifications Induced in 316L Steel by Laser Peening and Shot-Peening. Influence on pitting Corrosion Resistance, *Mater. Sci. Eng. A*, 2000, **280**, p 294–302
10. H.-S. Lee, D.-S. Kim, J.-S. Jung, Y.-S. Pyoun, and K. Shin, Influence of Peening on the Corrosion Properties of AISI, 304 Stainless Steel, *Corros. Sci.*, 2009, **51**, p 2826–2830
11. J. Lu, B. Han, C. Cui, C. Li, and K. Luo, Electrochemical and Pitting Corrosion Resistance of AISI, 4145 Steel Subjected to Massive Laser Shock Peening Treatment with Different Coverage Layers, *Opt. Laser Technol.*, 2017, **88**, p 250–262
12. C.Y. Cui, X.G. Cui, Y.K. Zhang, K.Y. Luo, Q. Zhao, J.D. Hu et al., Microstructure and Microhardness Analysis of the Hexagonal Oxides Formed on the Surface of the AISI, 304 Stainless Steel After Nd:YAG Pulsed Laser Surface Melting, *Appl. Surf. Sci.*, 2010, **256**, p 6782–6786
13. W. Pacquentin, N. Caron, and R. Oltra, Effect of Microstructure and Chemical Composition on Localized Corrosion Resistance of a AISI, 304L Stainless Steel After Nanopulsed-Laser Surface Melting, *Appl. Surf. Sci.*, 2015, **356**, p 561–573
14. Y. Ait Albrimi, A. Ait Addi, J. Douch, R.M. Souto, and M. Hamdani, Inhibition of the Pitting Corrosion of 304 Stainless Steel in 0.5 M Hydrochloric Acid Solution by Heptamolybdate Ions, *Corros. Sci.*, 2015, **90**, p 522–528
15. S. Canay, N. Hersek, A. Culha, and S. Bilgic, Evaluation of Titanium in Oral Conditions and Its Electrochemical Corrosion Behaviour, *J. Oral Rehabil.*, 1998, **25**, p 759–764
16. A. Döner and G. Kardaş, N-Aminorhodanine as an Effective Corrosion Inhibitor for Mild Steel in 0.5 M $H_2SO_4$, *Corros. Sci.*, 2011, **53**, p 4223–4232
17. P. Córdoba-Torres, T. Mesquita, and R. Nogueira, Toward a Better Characterization of Constant-Phase Element Behavior on Disk Electrodes from Direct Impedance Analysis: Methodological Considerations and Mass Transport Effects, *Electrochim. Acta*, 2013, **92**, p 323–334
18. N. Dai, L.-C. Zhang, J. Zhang, X. Zhang, Q. Ni, Y. Chen et al., Distinction in Corrosion Resistance of Selective Laser Melted Ti-6Al-4V Alloy on Different Planes, *Corros. Sci.*, 2016, **111**, p 703–710
19. Q.-Y. Wang, X.-Z. Wang, H. Luo, and J.-L. Luo, A Study on Corrosion Behaviors of Ni-Cr-Mo Laser Coating, 316 Stainless Steel and X70 Steel in Simulated Solutions with $H_2S$ and $CO_2$, *Surf. Coat. Technol.*, 2016, **291**, p 250–257
20. A.Y. Musa, A.A.H. Kadhum, A.B. Mohamad, A.A.B. Rahoma, and H. Mesmari, Electrochemical and Quantum Chemical Calculations on 4,4-dimethyloxazolidine-2-thione as Inhibitor for Mild Steel Corrosion in Hydrochloric Acid, *J. Mol. Struct.*, 2010, **969**, p 233–237
21. N. Zaveri, M. Mahapatra, A. Deceuster, Y. Peng, L. Li, and A. Zhou, Corrosion Resistance of Pulsed Laser-Treated Ti-6Al-4V Implant in Simulated Biofluids, *Electrochim. Acta*, 2008, **53**, p 5022–5032
22. M. Muralisankar, R. Sreedharan, S. Sujith, N.S.P. Bhuvanesh, and A. Sreekanth, N(1)-pentyl isatin-N(4)-methyl-N(4)-phenyl thiosemicarbazone (PITSc) as a Corrosion Inhibitor on Mild Steel in HCl, *J. Alloys Compd.*, 2017, **695**, p 171–182
23. C.Y. Cui, X.G. Cui, Y.K. Zhang, Q. Zhao, J.Z. Lu, J.D. Hu et al., Microstructure and Corrosion Behavior of the AISI, 304 Stainless Steel After Nd:YAG Pulsed Laser Surface Melting, *Surf. Coat. Technol.*, 2011, **206**, p 1146–1154
24. W. Pacquentin, N. Caron, and R. Oltra, Nanosecond Laser Surface Modification of AISI, 304L Stainless Steel: Influence the Beam Overlap on Pitting Corrosion Resistance, *Appl. Surf. Sci.*, 2014, **288**, p 34–39
25. A. Singh, Y. Lin, I.B. Obot, E.E. Ebenso, K.R. Ansari, and M.A. Quraishi, Corrosion Mitigation of J55 Steel in 3.5% NaCl Solution by a Macrocyclic Inhibitor, *Appl. Surf. Sci.*, 2015, **356**, p 341–347
26. A.Y. Musa, R.T. Jalgham, and A.B. Mohamad, Molecular Dynamic and Quantum Chemical Calculations for Phthalazine Derivatives as Corrosion Inhibitors of Mild Steel in 1M HCl, *Corros. Sci.*, 2012, **56**, p 176–183
27. V. Antonov, I. Iordanova, and S. Gurkovsky, Investigation of Surface Oxidation of Low Carbon Sheet Steel During Its Treatment with Nd: Glass Pulsed Laser, *Surf. Coat. Technol.*, 2002, **160**, p 44–53
28. P. Behjati, A. Kermanpur, A. Najafizadeh, H.S. Baghbadorani, J.-G. Jung, and Y.-K. Lee, Enhanced Mechanical Properties in a High-Manganese Austenitic Steel Through Formation of Nano Grains, Nano Twinned Austenite Grains, Nano Carbides and TRIP, *Mater. Sci. Eng. A*, 2014, **610**, p 273–278
29. H.H. Colin, Cast Iron, *Corrosion: Metal/Environment Reactions*, 2nd ed., L.L. Shrier, Ed., Newnes, 1976, p 3:85–3:97
30. R.A. Antunes, R.U. Ichikawa, L.G. Martinez, and I. Costa, Characterization of Corrosion Products on Carbon Steel Exposed to Natural Weathering and to Accelerated Corrosion Tests, *Int. J. Corros.*, 2014, **2014**, p 419570
31. A. Momber, Colour-Based Assessment of Atmospheric Corrosion Products, Namely of Flash Rust, on Steel, *Mater. Corros.*, 2012, **63**, p 333–342
32. J. Schneider and M.S. Chatterjee, Introduction to Surface Hardening of Steels, *ASM Handbook, Vol. 4A, Steel Heat Treating Fundamentals and Processes*, J. Dossett and G.E. Totten, Ed., ASM International, Materials Park, 2013, p 389–397